ELSEVIER

Journal of Photochemistry and Photobiology A: Chemistry 148 (2002) 331–339

Journal of Photochemistry and Photobiology A:Chemistry

www.elsevier.com/locate/jphotochem

Light-induced super-hydrophilicity and photocatalytic activity of mesoporous TiO_2 thin films

Jimmy C. Yu [a,*], Jiaguo Yu [a,b], Wingkei Ho [a], Jincai Zhao [c]

[a] *Department of Chemistry and Materials Science and Technology Research Centre, The Chinese University of Hong Kong, Shatin, New Territories, Hong Kong, Hong Kong*

[b] *State Key Lab of Advanced Technology for Materials Synthesis and Processing, Wuhan University of Technology, Wuhan 430070, China*

[c] *The Laboratory of Photochemistry, Center for Molecular Science, Institute of Chemistry, The Chinese Academy of Sciences, Beijing 100080, China*

Received 24 July 2001; received in revised form 4 September 2001; accepted 4 September 2001

Abstract

Transparent mesoporous TiO_2 ($MTiO_2$) and TiO_2 nanometer thin films were prepared on fused quartz via the modified reverse micellar and sol–gel methods. The $MTiO_2$ and TiO_2 films were characterized by X-ray photoelectron spectroscopy (XPS), atomic force microscopy (AFM), X-ray diffraction (XRD), BET surface area and UV–Vis spectrophotometry. The photoinduced super-hydrophilicity and photocatalytic activity of the films were evaluated by the water contact angle measurement and photocatalytic oxidation of acetone in air, respectively. It was found that $MTiO_2$ thin films at 500 °C showed higher photocatalytic activity and better light-induced hydrophilicity than the TiO_2 thin films. This is attributed to the following reasons: (1) $MTiO_2$ thin films are composed of smaller monodisperse spherical particles about 15 nm diameter, and possess more mesopores between spherical particles and higher surface areas and surface roughness, (2) the monodispersity of $MTiO_2$ particles was beneficial to the transfer and separation of photo-generated electrons and holes inside of and on the surface of TiO_2 particles, and reduced the recombination of photo-generated electrons and holes. At 900 °C, the $MTiO_2$ and TiO_2 films appeared to be in the rutile phase, but showed photoinduced hydrophilicity and no photocatalytic activity. This confirmed that the mechanism of photoinduced super-hydrophilicity of the films is different from that of photocatalytic oxidation.

Keywords: Mesoporous TiO_2 thin films; Modified reverse micellar method; Anatase; Rutile; Photocatalytic activity; Photoinduced hydrophilicity

1. Introduction

Among various oxide semiconductor photocatalysts, titania appears to be a promising and important prospect for use in environmental purification, because of its strong oxidizing power, photoinduced hydrophilicity, nontoxicity and long-term photostability [1–3]. Besides the usual photocatalytic activity, photoinduced super-hydrophilic properties of the surface of TiO_2 polycrystalline thin films have attracted much attention in recent years. By utilizing this photocatalytically active and super-hydrophilic surface of TiO_2, we can develop anti-fogging or self-cleaning glass, mirrors and other ecological building materials. However, the photocatalytic activity and photoinduced hydrophilicity must be further enhanced for practical uses. For the purposes of achieving this, it is of great importance to improve the methods of preparing titania. The preparation of mesoporous TiO_2 ($MTiO_2$) thin film by reverse micelle method is not a new concept. Stathatos et al. [4,5] first reported the preparation of $MTiO_2$ thin film by this method and photocatalytically deposited silver nanoparticles on titania nanoparticle films. However, this method has a serious limitation—the stability of TiO_2 sol is poor and will become gel in a short time (a few hours). In order to overcome this disadvantage, we added a small amount of acetylacetone to the reverse micelle solution and the stability of TiO_2 sol was greatly improved.

Usually, TiO_2 colloidal suspensions or films are prepared by hydrolysis of alkoxide precursors in an aqueous or alcoholic environment. However, reverse micelles provide a means to control the size, size-polydispersity and shape of TiO_2 nanoparticles, not only in suspensions but also in films [4,5]. Formation of $MTiO_2$ films by reverse micelles involves three stages [4]: (1) hydrolysis of an alkoxide in a reverse micellar environment and formation of a gel by inorganic polymerization; (2) deposition of a composite inorganic/organic film on a solid substrate; (3) heating of the film up to 450–500 °C to burn out all organic content and to obtain the final mesoporous structure. The resulting $MTiO_2$

* Corresponding author. Tel.: +852-26096268; fax: +852-26035057.
E-mail address: jimyu@cuhk.edu.hk (J.C. Yu).

1010-6030/02/$ – see front matter
PII: S1010-6030(02)00060-6

thin films have high crystallinity and large surface area, which satisfies the basic requirements for photoactive TiO_2 films. Therefore, using reverse micelles should be a most promising method for making highly photoactive TiO_2 films.

This is the first report on the comparative studies of photocatalytic activity, photoinduced hydrophilicity and surface microstructures of $MTiO_2$ and TiO_2 thin films prepared by modified reverse micellar method and sol–gel route. A comparison of mesoporous TiO_2 films with conventionally prepared TiO_2 films will show the importance of the preparation method in the development of materials with novel properties.

2. Experimental

2.1. Preparation

All chemicals used in the present work were from Aldrich and were used as received. Millipore water was used in all experiments.

$MTiO_2$ thin films were prepared by using an improved method based on that of Lianos and coworkers [4,5]. The method was improved by adding acetylacetone to the reverse micellar solution in order to increase its stability. The obtained reverse micellar solution can be kept for at least a month. The preparation of the solution consisted of the following steps. Firstly, triton X-100 (26 g) and cyclohexane (150 ml) were mixed to form a reverse micellar solution under vigorous stirring. After 0.5 h, 1.08 g water was added to the solution at room temperature. The solution was turbid; however, it cleared out upon addition of titanium isopropoxide (23 g) [5]. The alkoxide solution was stirred at room temperature for hydrolysis reaction for 1 h. Finally, 10 ml acetylacetone was added to the above solution, resulting in a stable TiO_2 sol. The concentration of triton X-100, titanium isopropoxide, acetylacetone and water was 0.2, 0.4, 0.2 and 0.3 M, respectively. The $MTiO_2$ films formed on quartz (80 mm × 30 mm × 2 mm) were prepared from the above TiO_2 sol solution by dipping–withdrawing in an ambient atmosphere. The quartzes coated with TiO_2 gel films were heat-treated in air at a rate of 3 °C/min up to 500 °C and were left to stay in the furnace at the highest temperature for about 1 h. The withdrawal speed was 4 mm s^{-1}. The thickness of the TiO_2 films was adjusted by repeating the cycle from dipping to heat treatment. In order to obtain TiO_2 films with different phase structures, the above films were heat-treated at 900 °C for 1 h, respectively.

Precursor solutions for TiO_2 films were prepared by the following method [6]. Titanium isopropoxide and triethanolamine were dissolved in ethanol. After stirring vigorously for 1 h at room temperature, the mixture of water and ethanol was added dropwise to the solution under vigorous stirring. The resultant alkoxide solution was kept at room temperature for hydrolysis reaction for 2 h, resulting in the TiO_2 sol. The chemical composition of the resulting alkoxide solution was $Ti(OC_3H_7)_4$:C_2H_5OH:H_2O:$N(C_2H_4OH)_3$ = 1:26.5:1:1 in molar ratio. The other conditions and post-treatment processing are the same as those of $MTiO_2$ films.

Apart from the above-described thin film samples, powder samples were also prepared with the same procedure as the thin films. The detailed process was as follows: firstly, TiO_2 reverse micelle sol, or TiO_2 sol which had the same composition as the thin film samples, was dried at 100 °C in air in order to obtain gels, then heat-treated at a rising rate of 3 °C/min up to and at 500 °C for 1 h in air, and finally ground by agate mortar to obtain $MTiO_2$ and TiO_2 powders.

2.2. Characterization

Surface roughness and morphologies of various TiO_2 thin films were evaluated by atomic force microscopy (AFM: Nano Scope 3a, Digital Instruments, Santa Barbara, CA), The X-ray diffraction (XRD) patterns obtained on a Philips MPD 18801 X-ray diffractometer using Cu Kα radiation at a scan rate of 0.05° 2θ S^{-1} were used to determine the identity of any phases present and their crystallite size. The accelerating voltage and the applied current were 35 kV and 20 mA, respectively. The crystallite size was calculated by X-ray line broading analysis by Scherrer formula. UV–Vis spectra of films were obtained using a UV–Vis spectrophotometer (Cary 100 Scan Spectrophotometers, Varian, USA). X-ray photoelectron spectroscopy (XPS) measurements were performed on a PHI Quantum 2000 XPS System with a monochromatic Al Kα source and a charge neutralizer; all the binding energies were referenced to the C 1s peak at 284.8 eV of the surface adventitious carbon. The film thickness was measured using cross-sectional observation of scanning electron microscopy (SEM: Hitachi, S-450, Japan) and surface profiler (Alpha-step 500, Tencor Instrument, USA). The Brunauer–Emmett–Teller (BET) surface area (S_{BET}) and pore parameters of the powder samples were determined by nitrogen adsorption–desorption isotherm measurements at 77 K on a Micromeritics ASAP 2000 nitrogen adsorption apparatus. All the samples measured were degassed at 180 °C before the actual measurements. Pore size distributions were calculated from desorption branch of the isotherm by the Barrett–Joyner–Halenda (BJH) method using the Halsey equation.

2.3. Measurements of photocatalytic activity and photoinduced super-hydrophilicity

The photocatalytic activity experiments on film photocatalysts for the oxidation decomposition of acetone in air were performed at ambient temperature using a 7000 ml reactor. The detailed experimental process can be found in reference [7]. During the photocatalytic reaction, a near 3:1 ratio of carbon dioxide products to acetone destroyed was observed, and the acetone concentration decreased steadily with increase in ultraviolet (UV) illumination time. Each reaction

was followed for 60 min. The photocatalytic oxidation of acetone is a pseudo-first-order reaction and its kinetics may be expressed as follows [8]: $\ln(C_0/C) = kt$, where k is the apparent rate constant of pseudo-first-order, C_0 and C the initial concentration and reaction concentration of acetone, respectively.

The photoinduced hydrophilicity of thin films was evaluated by examining the change of water contact angle before and after illuminating with a 15 W 365 nm UV lamp (Cole-Parmer Instrument) in an ambient environment. The intensity of UV light striking the films was about 540 ± 10 μW/cm^2. The sessile drop method was used for contact angle measurements with a contact angle meter (Cam-Micro, Tantec, USA). The experimental error of the measurements was ±1°. The droplet size used for the measurements was 5 ml. Water droplets were placed at five different positions for one sample and the average value was adopted as the contact angle.

3. Results and discussion

3.1. Characterizations of materials

Fig. 1 shows the UV–Vis absorption spectra of $MTiO_2$ at 500 °C (a) and 900 °C (c) and TiO_2 films at 500 °C (b) deposited on quartz by one coating cycle. It can be seen from Fig. 1 that the preparation method and phase structure of thin films influence the transmittance spectra. The transmittance of $MTiO_2$ film at 500 °C is the highest, over 85% over the entire visible light spectral region. The fast decrease below 380 nm is due to absorption of light caused by the excitation of electrons from the valence band to the conduction band of TiO_2. The oscillation of the curves between 800 and 380 nm is due to the interference between the film and the substrate. Compared with the transmittance spectra of TiO_2 film, the absorption edge of $MTiO_2$ films shows a slight pseudo-blue

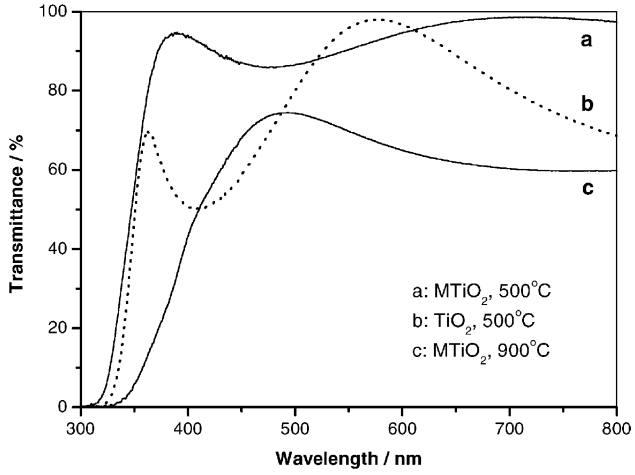

Fig. 1. UV–Vis absorption spectra of $MTiO_2$ and TiO_2 films deposited on quartz by one coating cycle: (a) $MTiO_2$ at 500 °C, (b) TiO_2 at 500 °C and (c) $MTiO_2$ at 900 °C.

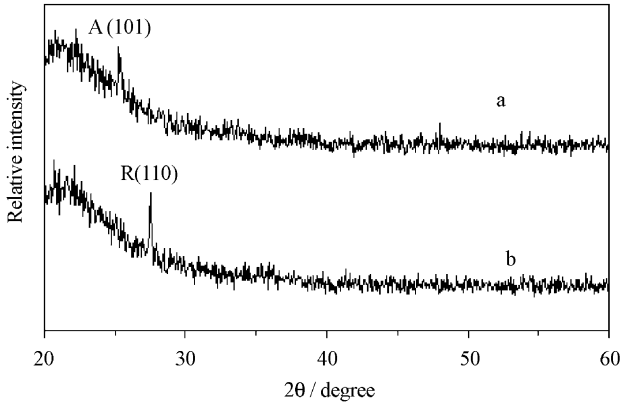

Fig. 2. XRD patterns of $MTiO_2$ films deposited on quartz and heat-treated at (a) 500 °C and (b) 900 °C.

shift. This is ascribed to the fact that $MTiO_2$ film contains smaller TiO_2 particles, and a quantum size effect appears, resulting in a pseudo-blue shift of the absorption edge. The difference in transmittance between $MTiO_2$ and TiO_2 films was attributed to the difference in film thickness and absorption of light. The thickness of these films ranges between 160 and 180 nm. When $MTiO_2$ thin film was heat-treated at 900 °C, its transmittance decreased greatly, and the adsorption edge shows a significant red shift. The former is attributable to $MTiO_2$ film at 900 °C being composed of larger particles (as shown in Fig. 3), which causes scattering of light, while the latter is attributable to $MTiO_2$ film at 900 °C with rutile phase structure owing to the bandgap of rutile less than that of anatase.

Fig. 2 shows XRD patterns of $MTiO_2$ films deposited on quartz and heat-treated at (a) 500 °C and (b) 900 °C. At 500 °C, $MTiO_2$ film exhibits anatase phase structure, while at 900 °C, it is completely transformed into rutile structure. It is obvious that the anatase and rutile $MTiO_2$ films exhibit preferential orientation in (1 0 1) and (1 1 0) peaks, respectively. The average crystallite size of $MTiO_2$ films, shown in Table 1, was calculated using the line broadening methods and the equation proposed by Scherrer [7]. XRD results of TiO_2 films at 500 and 900 °C are similar to those of $MTiO_2$ films.

Fig. 3 shows two-dimensional and three-dimensional AFM images of the $MTiO_2$ and TiO_2 thin films deposited on quartz by one coating cycle at 500 and 900 °C. At 500 °C, the surface morphologies and roughness of $MTiO_2$ and TiO_2 films are obviously different. Fig. 3a and b shows that $MTiO_2$ film prepared by the modified reverse micellar method and calcined at 500 °C is composed of monodisperse spherical particles of about 15 nm diameter and has a mesoporous structure between monodisperse TiO_2 particles [4]. Monodispersity is an advantage of the reverse micellar method for the synthesis of TiO_2 nanoparticles by hydrolysis of titanium isopropoxide [4,5]. This hydrolysis process competes with the hydration of surfactant polar heads for water molecules. Restructuring of surfactant molecules

Table 1
Preparation conditions and physicochemical properties of $MTiO_2$ and TiO_2 films[a]

No.	Composition	Thickness (μm)	Calcination temperature (°C)	Phase structure	Crystallite size (nm)	R_{rms} (nm)	OH before UV illumination (%)	OH after UV illumination (%)
A	$MTiO_2$	0.17	500	Anatase	13.1	1.04	10.8	14.6
B	TiO_2	0.18	500	Anatase	15.6	0.56	8.7	11.9
C	$MTiO_2$	0.16	900	Rutile	107.3	11.11	7.6	9.8
D	TiO_2	0.17	900	Rutile	113.2	5.16	6.6	8.9

[a] All film samples deposited on quartz by one coating cycle.

around the polar species formed during hydrolysis results in growth limitations and uniform particles sizes [5]. It can also be seen from Fig. 3c and d that the TiO_2 film prepared by sol–gel route and calcined at 500 °C also has granular microstructure and is composed of about 80 nm spherical particles. According to the previous XRD results, these 80 nm particles on the surface of TiO_2 thin films are aggregates of many small TiO_2 crystallites. In addition to particle diameter, AFM image analysis also gives the values of surface roughness. The root mean square roughness values (R_{rms}) of $MTiO_2$ and TiO_2 are 1.04 and 0.56 nm, respectively. Fig. 3b and d also shows that the surface morphology of $MTiO_2$ film is rougher than that of TiO_2 film.

At 900 °C, the surface morphology and roughness of $MTiO_2$ and TiO_2 films are changed significantly owing to phase transformation of anatase to rutile and sintering and

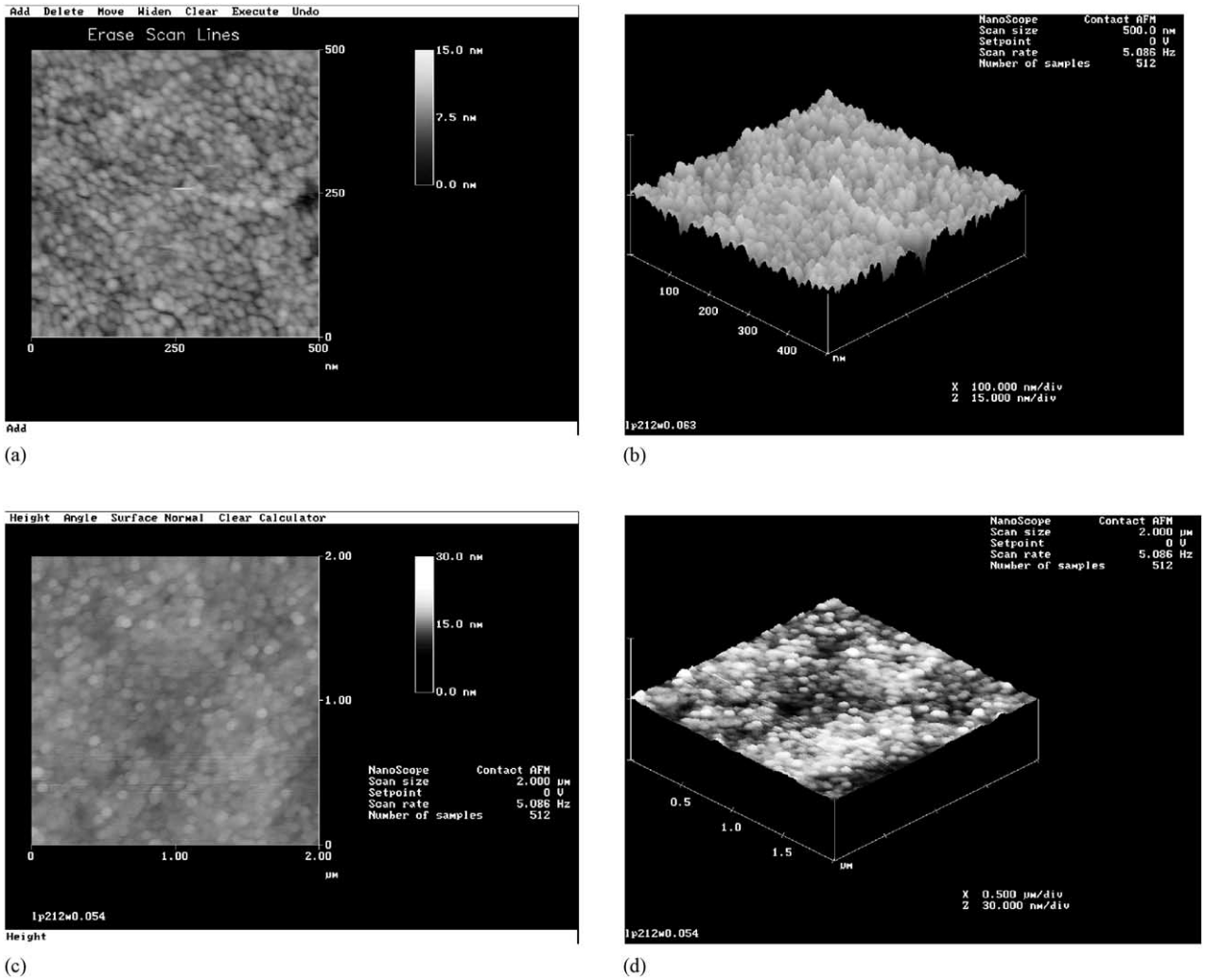

Fig. 3. Two-dimensional and three-dimensional AFM images of the surface of $MTiO_2$ and TiO_2 thin films deposited on quartz by one coating cycle at 500 and 900 °C. (a and b) $MTiO_2$ at 500 °C, (c and d) TiO_2 at 500 °C, (e and f) $MTiO_2$ at 900 °C and (g and h) TiO_2 at 900 °C.

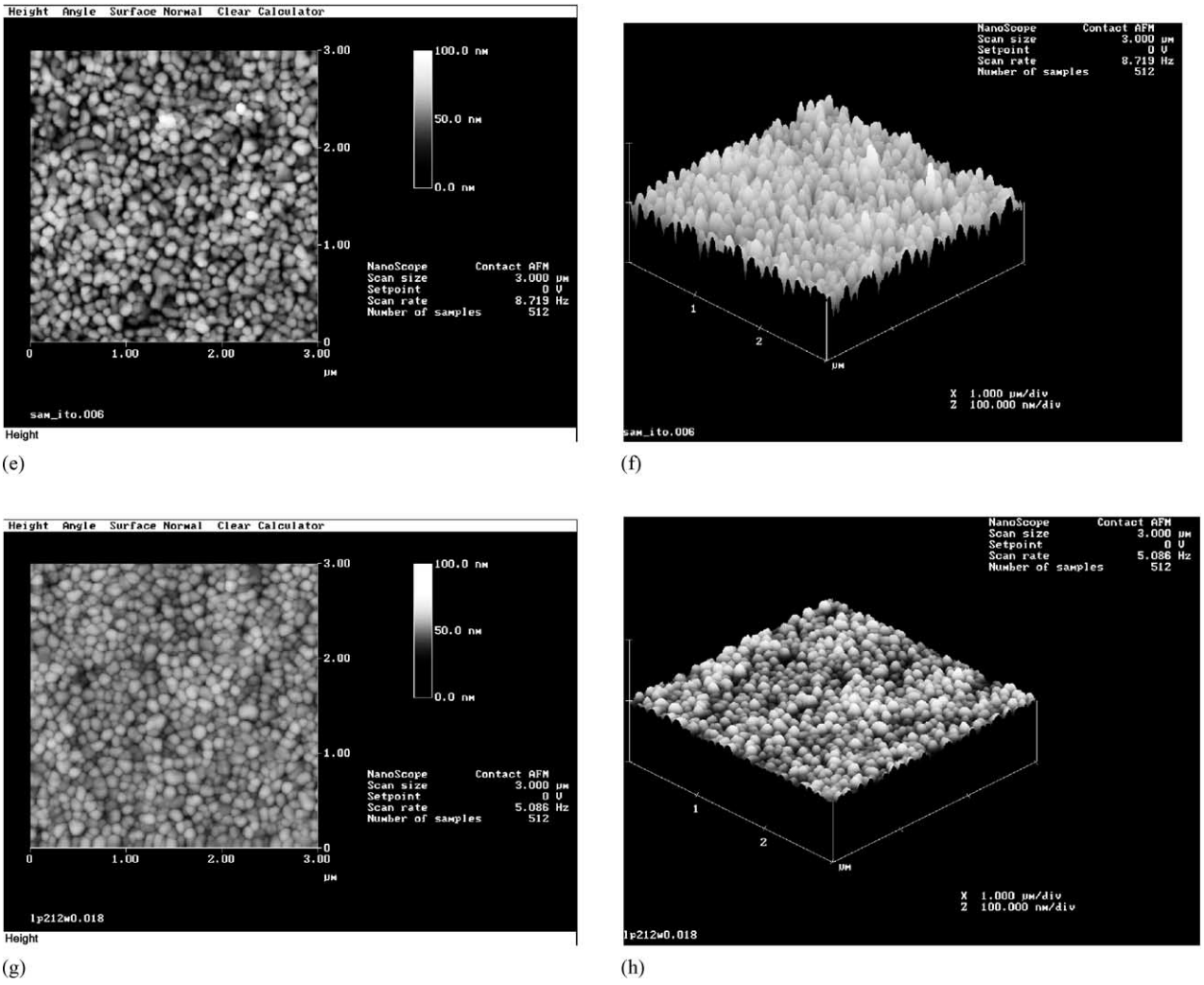

Fig. 3. (*Continued*).

growth of TiO_2 crystallites. Fig. 3e and f shows that the $MTiO_2$ film at 900 °C is composed of about 100 nm sphere particles. Although TiO_2 film at 900 °C is also composed of about 110 nm sphere particles (Fig. 3g and h), there are obvious differences between the surface microstructures of $MTiO_2$ and TiO_2 films at 900 °C. $MTiO_2$ film contains obvious pore structures between particles, hence the roughness and R_{rms} value of $MTiO_2$ films at 900 °C is larger than that of TiO_2 film at 900 °C as shown in Fig. 3 and Table 1. The surface morphologies of $MTiO_2$ and TiO_2 films at 900 °C are much clearer than those at 500 °C. This is probably due to the difference in phase structure and heat-treatment temperature of the films.

The BET surface areas of $MTiO_2$ and TiO_2 thin films on quartz could not be measured directly by nitrogen adsorption apparatus, because the amount of the thin films on quartz was too small. We measured the BET surface areas of powder samples prepared through the same procedure as the thin films. Fig. 4 shows the pore size distribution curve calculated from desorption branch of nitrogen isotherm by the BJH method using the Halsey equation. The inset shows the corresponding nitrogen adsorption–desorption isotherms of $MTiO_2$ powders prepared from TiO_2 reverse micellar solution and calcined at 500 °C for 1 h. The sharp decline in desorption curve is indicative of mesoporosity, the pore size distribution calculated from the desorption branch of the nitrogen isotherm by the BJH method shows that an average pore size of 3.59 nm. The pore diameter distribution is narrow and the range of pores is 2.5–6.0 nm. The BET surface area and pore parameters of $MTiO_2$ and TiO_2 powders determined from nitrogen adsorption–desorption isotherm by the BJH method are summarized in Table 2. The pore size distribution curve and nitrogen adsorption and desorption isotherms of TiO_2 powders (not shown here) are different from those of $MTiO_2$ powders. The BET surface area of TiO_2 powders is much smaller than that of $MTiO_2$ powders. Moreover, the pore size distribution is very wide, ranging from 1.5 to 70 nm. It can also be seen from Table 2 that porosity and pore volume of $MTiO_2$ powders are larger than those of TiO_2 powders. With increasing calcination temper-

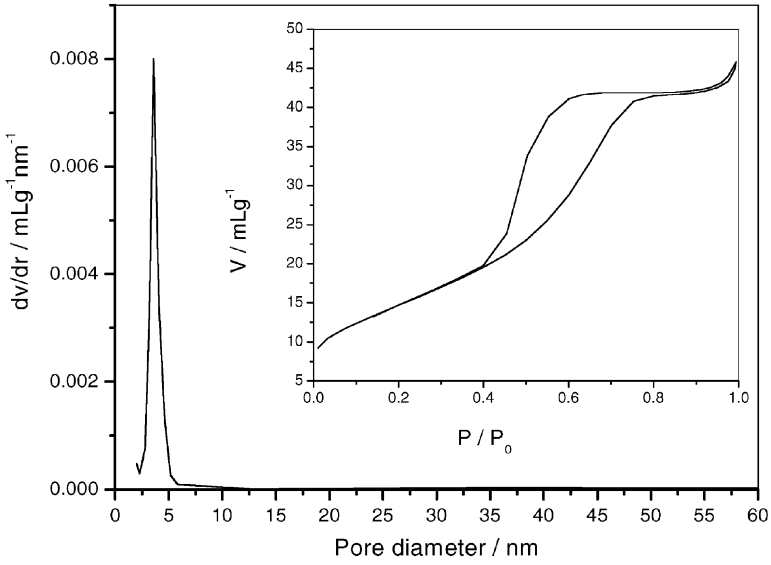

Fig. 4. Pore size distribution curve calculated from desorption branch of the nitrogen isotherm by the BJH method. Inset: the corresponding nitrogen adsorption–desorption isotherms of $MTiO_2$ powders prepared from reverse micelle TiO_2 solution and calcined at 500 °C for 1 h.

ature, TiO_2 crystallites rapidly grow and BET surface areas decrease drastically. At 700 °C, BET surface area of $MTiO_2$ powders drops to about 1 $m^2\,g^{-1}$. At 900 °C, BET surface area becomes negligibly small.

Fig. 5 shows the high resolution XPS spectra of the O 1s region, taken on the surface of $MTiO_2$ film (a) before and (b) after UV illumination. Before UV illumination, the O 1s region consists of two peaks (dashed line). The 529.90 eV peak corresponds to Ti–O in TiO_2, and the 531.90 eV peak is related with the hydroxyl groups. After UV illumination, the peak for hydroxyl groups increases significantly. Table 1 lists the changes of hydroxyl content on the surface of $MTiO_2$ and TiO_2 films before and after UV illumination. The hydroxyl content (%) is the ratio of the area of 531.90 eV peak to the total area of the two O 1s peaks. The hydroxyl contents in all samples after UV illumination are greater than those before UV illumination. This is because some water molecules dissociatively adsorbed on the defective sites of TiO_2 film surfaces [2]. The hydroxyl groups detected by XPS on the film surfaces were the chemisorbed H_2O. Although some H_2O is physically adsorbed on the surface of TiO_2 films, the physisorbed H_2O on TiO_2 is easily desorbed under the ultra-high vacuum condition of the XPS system. Therefore, the XPS spectra do not shows the physisorbed H_2O on the surface of TiO_2 films. Table 1 also shows that the hydroxyl content of $MTiO_2$ thin films is greater than that of TiO_2 thin films in both anatase and rutile samples. This was ascribed to the fact that $MTiO_2$ films contain smaller crystallites, more mesopores, greater specific surface area and higher surface roughness [9].

3.2. Photocatalytic activity

It can be seen from Table 3 that, at 500 °C, photocatalytic activity of $MTiO_2$ thin films prepared by the modified reverse micellar method is obviously higher than that of TiO_2 thin films prepared by the sol–gel route. The apparent rate constant, degradation rate and specific photocatalytic activity of $MTiO_2$ film are greater than those of TiO_2 film by up to more than two times. Characterization results of AFM, UV–Vis spectra, XRD and XPS can explain the enhancement in photocatalytic activity. Firstly, AFM results show that the particle size in $MTiO_2$ thin films is about 1/5 of that of TiO_2 films. Therefore, $MTiO_2$ thin films possess much larger surface area (as shown in Table 2). Generally, the photodegradation rates of chemical compounds on semiconduc-

Table 2
BET surface areas and pore parameters of $MTiO_2$ and TiO_2 powders at 500 °C

No.	Composition	S_{BET}[a] ($m^2\,g^{-1}$)	Porosity[b]	Pore volume[c] ($ml\,g^{-1}$)	Pore size[d] (nm)
A	$MTiO_2$	53.2	20.8	0.067	3.59
B	TiO_2	9.1	9.8	0.029	6.52

[a] BET surface area calculated from the linear part of the BET plot ($P/P_0 = 0.05$–0.3).
[b] The porosity is estimated from the pore volume determined using the adsorption branch of the N_2 isotherm curve at the $P/P_0 = 0.995$ single point.
[c] Total pore volume taken from the volume of N_2 adsorbed at $P/P_0 = 0.995$.
[d] Average pore diameter, estimated using the adsorption branch of the isotherm and the BJH formula.

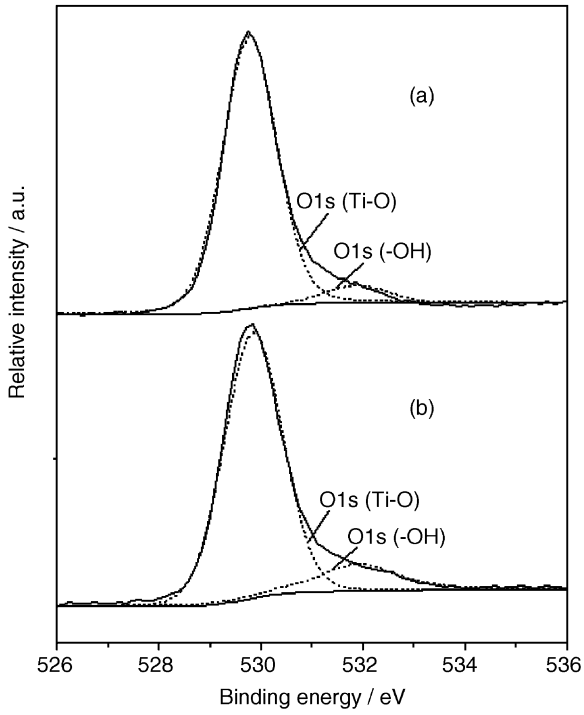

Fig. 5. High resolution XPS spectra of the O 1s region for the surface of $MTiO_2$ films: (a) before and (b) after UV illumination.

tor surfaces follow classical Langmuir–Hinshelwood (LH) kinetic expression [1,2,8]: $r = k\theta = kKc/(1 + Kc)$, where the rate is proportional to the coverage θ or the adsorption constant K. Hence a high coverage θ or a large adsorption constant K would result in a high photocatalytic activity. Furthermore, the monodispersity of TiO_2 particles on the surface of $MTiO_2$ films is probably beneficial to the transfer and separation of photo-generated electrons and holes inside of and on the surface of TiO_2 particles, and reduces the recombination of photo-generated electrons and holes. Of course, the higher porosity in $MTiO_2$ thin films is also beneficial to rapid diffusion of various reactants and products during UV illumination and enhances the speed of photocatalytic reaction. Secondly, UV–Vis spectra show that the absorption edge of $MTiO_2$ films is at a shorter wavelength range than that of TiO_2 film. This is because $MTiO_2$ films contain smaller crystallites of slightly higher bandgap energy and a stronger oxidation power [3]. XRD measurements further confirm that the crystallite size of $MTiO_2$ films is smaller than that of TiO_2 films. Finally, XPS results show that $MTiO_2$ thin films contain more hydroxyl groups. Of course, the increase in surface hydroxyl content will trap more photo-generated holes and thus prevent electron–hole recombination [10]. All these factors can enhance the photocatalytic activity of $MTiO_2$ thin films prepared by the modified reverse micellar method. On the other hand, at 900 °C, $MTiO_2$ and TiO_2 films showed negligible photocatalytic activity, this is due to, at 900 °C, $MTiO_2$ and TiO_2 films appearing to be in the rutile phase.

3.3. Photoinduced super-hydrophilicity

All our freshly prepared $MTiO_2$ and TiO_2 thin films on quartz showed highly hydrophilic property, their water contact angles were 5–15°. This was caused by the defects on the surface of the as-prepared TiO_2 thin films by high temperature calcination [11]. However, when these films were stored in dark rooms in air for 2 months, the water contact angle tended to increase up to certain saturation contact angle values about 50–60°. This is ascribed to the fact that the surface defective sites can be healed or replaced gradually by oxygen atoms, which cause the surface wettability to convert from hydrophilic to hydrophobic. From the viewpoint of practical use, the hydrophilicity of the films should remain stable for a long time, but this state is very difficult to reach. Fortunately, the water contact angles can be fully recovered to the original state and even reach 0° by UV illumination again [2]. Fig. 6 shows time dependence of water contact angle of $MTiO_2$ and TiO_2 films under UV irradiation of 540 μW/cm^2 in ambient conditions. As expected, sample A has the best photoinduced super-hydrophilicity. Its water contact angle drops from 61° to 0° within 30 min. While the photoinduced super-hydrophilicity of sample D is the worst. In order to further quantitatively characterize the conversion kinetics from hydrophobic to hydrophilic state of the films, the hydrophilicizing rates ($\Delta\theta$) of the films in the first 20 min under UV illumination were compared. As shown in Fig. 7, the hydrophilicizing rate ($\Delta\theta$) of sample A is about 3.0 °/min, while that of sample D is only 1.1 °/min.

The mechanism of photoinduced super-hydrophilicity of TiO_2 has been intensively investigated by many researchers

Table 3
Photocatalytic activity of $MTiO_2$ and TiO_2 thin films at 500 and 900 °C

No.	Composition	Thickness (μm)	Calcination temperature (°C)	Degradation rate[a] (%)	Rate constant $K \times 10^{-3}$ (min^{-1})	Specific photoactivity[b] (mol g^{-1} h^{-1})
A	$MTiO_2$	0.17	500	10.3	2.01	3.85×10^{-3}
B	TiO_2	0.18	500	4.8	0.762	1.88×10^{-3}
C	$MTiO_2$	0.16	900	Negligible	Negligible	Negligible
D	TiO_2	0.17	900	Negligible	Negligible	Negligible

[a] The area of quartz covered by the $MTiO_2$ and TiO_2 layer is about 140 cm^2, average degradation rate (C/C_0) of acetone after 1 h of photocatalytic reaction.

[b] Acetone degradation amount per unit mass catalyst after 1 h of photocatalytic reaction.

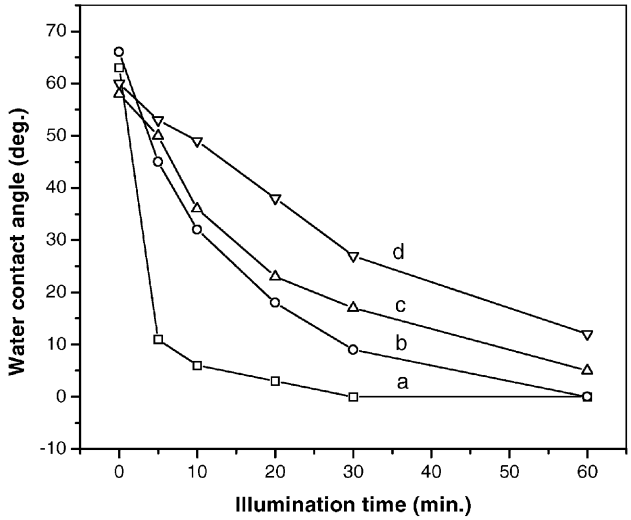

Fig. 6. Time dependence of water contact angle of $MTiO_2$ film at 500 °C (a), TiO_2 film at 500 °C (b), $MTiO_2$ film at 900 °C (c) and TiO_2 film at 900 °C (d) under UV irradiation for 1 h. The intensity of UV irradiation was 540 μW/cm^2 under ambient conditions (i.e. 295 K, 60% RH).

[11–15]. It was revealed from the studies by friction force microscopy (FFM), Fourier transform infrared spectroscopy (FT-IR), and XPS that preferential adsorption of water molecules on the photo-generated surface defective sites led to the formation of highly hydrophilic TiO_2 thin films surface [11–15]. The formation processes of defective sites on TiO_2 surface can be expressed as follows [11]:

$$TiO_2 + 2h\nu \rightarrow 2h^+ + 2e^- \quad (1)$$

$$O^{2-} + 2h^+ \rightarrow \tfrac{1}{2}O_2 + \square\,(\text{oxygen vacancy}) \quad (2)$$

$$Ti^{4+} + e^- \rightarrow Ti^{3+}\,(\text{surface trapped electron}) \quad (3)$$

In air, the surface trapped electrons tend to react immediately with O_2 adsorbed on the surface to form O_2^- or O_2^{2-} ions. Meanwhile, water molecules may coordinate into the oxygen vacancy sites (□), which leads to dissociative adsorption of the water molecules on the surface [11,15]. This process gives rise to the increase of hydroxyl content on the illuminated TiO_2 thin film surfaces.

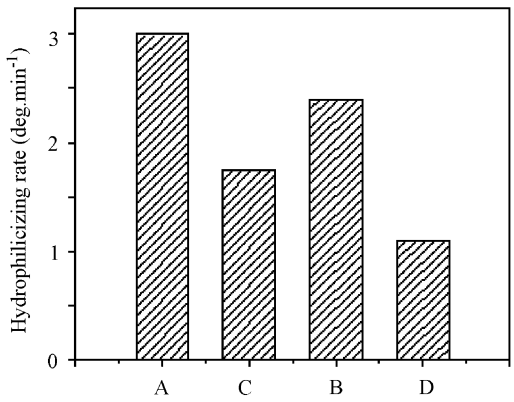

Fig. 7. Hydrophilicizing rate of $MTiO_2$ and TiO_2 thin films calcined at 500 and 900 °C. A: $MTiO_2$ at 500 °C, B: TiO_2 at 500 °C, C: $MTiO_2$ at 900 °C and D: TiO_2 at 900 °C.

The difference of hydrophilicizing rate of $MTiO_2$ and TiO_2 thin films is attributable to the change in phase structure, surface morphology, surface hydroxyl content and specific surface area. For the films with identical phase structure, preparative methods obviously influence the hydrophilicizing rate ($\Delta\theta$) of the films. The hydrophilicizing rate ($\Delta\theta$) of samples prepared by modified reverse micelle method is greater than that of samples prepared by sol–gel route. This is because the films prepared by modified reverse micelle method have more mesopores and larger surface areas, which cause water molecules to coordinate into more easily the oxygen vacancy sites on the surface of $MTiO_2$ thin films and make the films appear better photoinduced super-hydrophilicity. It is well known that the wettability of solid surfaces with liquids is governed not only by the chemical properties of the surfaces but also by their geometry [16,17]. As far as the geometry of a surface is concerned, the hydrophilicity is known to be enhanced by fine roughness. Therefore, an increase in the roughness of the $MTiO_2$ thin film surfaces enhances their hydrophilic properties and decreases water contact angles. Of course, with increasing the content of chemisorbed –OH on the surface, the $MTiO_2$ thin film surface becomes more polar and hydrophilic. Furthermore, the mesoporous structure of samples A and C can also enhance their hydrophilicity owing to a two-dimensional capillary phenomenon [16,17].

For the films prepared by the same method, phase structure would affect the hydrophilicizing rate ($\Delta\theta$) of the films. The hydrophilicizing rate ($\Delta\theta$) of samples A and B with anatase structures is greater than that of samples C and D with rutile structure. This can be explained by the longer lifetime of photo-generated electrons and holes in anatase structure [1–3], resulting in the formation of more oxygen vacancies. Moreover, anatase films contain more hydroxyl content on the surface, which would also decrease water contact angle. Hence the rate of photoinduced super-hydrophilicity of rutile TiO_2 films is slower than that of anatase TiO_2 films under UV illumination. By comparing the photocatalytic activity and photoinduced super-hydrophilicity of anatase and rutile TiO_2 thin films, it was found that rutile TiO_2 thin film showed no photocatalytic activity, but it did exhibit photoinduced super-hydrophilicity. This further confirmed that the photoinduced super-hydrophilic mechanism of TiO_2 thin films was different from the mechanism of photocatalytic reaction.

4. Conclusions

Transparent $MTiO_2$ and TiO_2 thin films were prepared on fused quartz via the modified reverse micellar method and sol–gel route, and were characterized by XRD, AFM, XPS, BET and UV–Vis. The photoinduced hydrophilic-

ity and photocatalytic activity of the various film samples were investigated. The results obtained are summarized as follows:

(1) The photoinduced super-hydrophilicity and photocatalytic activity of $MTiO_2$ thin films at 500 °C is obviously higher than those of TiO_2 thin films. This is attributed to the fact that $MTiO_2$ thin film is composed of smaller monodisperse spherical particles. The monodispersity of TiO_2 particles is helpful in the transfer and separation of photo-generated electrons and holes in TiO_2 particles. $MTiO_2$ thin films with more mesopores and surface hydroxyl, higher surface area and roughness are also beneficial to the enhancement of photocatalytic activity and photoinduced super-hydrophilicity.
(2) Rutile TiO_2 thin film shows no photocatalytic activity, but it does exhibit photoinduced super-hydrophilicity. This is ascribed to the photoinduced super-hydrophilic mechanism of TiO_2 being different from the photocatalytic mechanism.
(3) Anatase phase and mesoporous structures can enhance photocatalytic activity and photoinduced super-hydrophilicity of films.

Acknowledgements

The work was partially supported by a grant from the National Natural Science Foundation of China and Research Grants Council of the Hong Kong Special Administrative Region, China (Project No. N_CUHK433/00 and 4001161947). This work was also financially supported by the Foundation for University Key Teachers of the Ministry of Education and the National Natural Science Foundation of China (50072016).

References

[1] M.R. Hoffmann, S.T. Martin, W. Choi, D.W. Bahnemann, Chem. Rev. 95 (1995) 69.
[2] A. Fujishima, T.N. Rao, D.A. Tryk, J. Photochem. Photobiol. C 1 (2000) 1.
[3] A.L. Linsebigler, G. Lu, J.T. Yates Jr., Chem. Rev. 95 (1995) 735.
[4] A.L.E. Stathatos, G.P. Lianos, J.T.F. DelMonte, D. Levy Jr., D. Tsiourvas, Langmuir 13 (1997) 4295.
[5] E. Stathatos, P. Lianos, Langmuir 16 (2000) 2398–2400.
[6] J. Yu, X. Zhao, Q. Zhao, Thin Solid Films 379 (2000) 7.
[7] J. Lin, J.C. Yu, D. Lo, S.K. Lam, J. Catal. 183 (1999) 368.
[8] A. Fernandez, G. Lassaletta, V.M. Jimenez, A. Justo, A.R. Gonzalez-Elipe, J.M. Herrmann, H. Tahiri, Y. Ait-Ichou, Appl. Catal. B 7 (1995) 49.
[9] H. Kominami, H. Kumamoto, Y. Kera, B. Ohtani, Appl. Catal. B 30 (2001) 329.
[10] D.F. Ollis, E. Pelizzetti, N. Serpone, Environ. Sci. Technol. 25 (1991) 1523.
[11] N. Sakai, A. Fujishima, T. Watanabe, K. Hashimoto, J. Phys. Chem. B 105 (2001) 3023.
[12] R. Wang, N. Sakai, A. Fujishima, T. Watanabe, K. Hashimoto, J. Phys. Chem. B 103 (1999) 2188.
[13] N. Sakai, R. Wang, A. Fujishima, T. Watanabe, K. Hashimoto, Langmuir 14 (1998) 5918.
[14] R. Wang, K. Hashimoto, A. Fujishima, M. Chikuni, E. Kojima, A. Kitamura, M. Shimohigoshi, T. Watanabe, Adv. Mater. 10 (1998) 135.
[15] R. Sun, A. Nakajima, N. Sakai, A. Fujishima, T. Watanabe, K. Hashimoto, J. Phys. Chem. B 105 (2001) 1984.
[16] A.W. Adamson, A.P. Gast, Physical Chemistry of Surfaces, 6th Edition, Wiley, New York, 1997 (Chapter X).
[17] J. Yu, X. Zhao, Q. Zhao, G. Wang, Mater. Chem. Phys. 68 (2001) 253.